Available online at www.sciencedirect.com

ScienceDirect

Solar Energy 125 (2016) 99–110

SOLAR ENERGY

www.elsevier.com/locate/solener

Characterization of the intraday variability regime of solar irradiation of climatically distinct locations

Philippe Lauret [a,*], Richard Perez [b], Luis Mazorra Aguiar [c], Emeric Tapachès [a], Hadja Maimouna Diagne [a], Mathieu David [a]

[a] *Laboratoire de Physique et Ingénierie Mathématique pour l'Energie et l'environnement (PIMENT), University of La Réunion, Campus du Moufia 15, Avenue René Cassin, 97715 Saint Denis Messag 9, France*

[b] *ASRC, The University at Albany, SUNY, United States*

[c] *University Institute for Intelligent Systems and Numerical Applications in Engineering, University of Las Palmas de Gran Canaria, Edificio Central del Parque Tecnológico, Campus de Tafira, 35017 Las Palmas de Gran Canaria, Spain*

Received 19 August 2015; received in revised form 22 November 2015; accepted 23 November 2015
Available online 28 December 2015

Communicated by: Associate Editor Jan Kleissl

Abstract

This paper investigates the relationship between two parameters characterizing a given location on a given day: the daily clear sky index KT^* and the intraday variability given by the standard deviation of the changes in the hourly clear sky index $\sigma(\Delta kt^*_{\Delta t})$. Empirical evidence assembled from twenty climatically distinct locations led us to derive a simple model to infer intraday variability from the day's clear sky index. Although the model shows little dependence on location, we did observe a systematic difference traceable to a location's prevailing cloud formation regime. Therefore, we also propose two alternative models for sites where cloud formations is influenced by local orography and sites where cloud formation is traceable to weather events only. Finally, we present a possible application of the models to enhance the informative content of day(s) ahead NWP forecasts.

Keywords: Solar resource; Solar irradiation; Variability; Model; NWP model

1. Introduction

The characterization of solar resource variability is an important issue for grid-connected solar PV as penetration increases because of the challenges variability poses to grid operators (Perez and Hoff, 2013).

The topic of solar energy variability has generated a considerable amount of research during these last years. In particular, much attention has been paid to the study of the short-term variability of the PV power output of a single plant due to the cloud fluctuations (Hansen, 2007; Marcos et al., 2011; Mills et al., 2010; Perpiñán et al., 2013; Van Haaren et al., 2014).

Some authors (Perez and Hoff, 2013; Lave et al., 2012; Sengupta and Keller, 2011; Murata et al., 2009) also showed that short-term power fluctuations generated by an ensemble of geographical dispersed PV plants are considerably reduced compared to a single one, and that the reduction can be predicted on the basis of power plant interdistance, cloud or cloud system motion and considered fluctuation time scale.

Metrics describing and quantifying variability at different time scales are a key ingredient of this characterization.

* Corresponding author. Tel.: +262 692 67 48 07; fax: +262 262 93 86 65.
E-mail address: philippe.lauret@univ-reunion.fr (P. Lauret).

http://dx.doi.org/10.1016/j.solener.2015.11.032
0038-092X/

Van Haaren et al. (2014) proposed a quantitative metric called the Daily Aggregate Ramp Rate (DARR) which sums 1-min single Plane Of Array (POA) irradiance sensor over each day to characterize daily variability in a utility-scale plant. Lenox and Nelson (2010) proposed the Inter-Hour Variability Score (IHVS) which summed the absolute value of 1-min changes in POA irradiance and AC power output in each hour. Badosa et al. (2013) showed that solar irradiance variability at the diurnal scale can be classified in regimes based on three parameters. These parameters are the daily clear-sky index, solar irradiance morning–afternoon asymmetry and random variability of the solar irradiance.

In a previous work, Perez et al. (2011) proposed models to characterize the one-minute intra-hourly solar variability based upon hourly inputs. Short-term variability metrics can be inferred by the model using hourly insolation data from e.g., satellite-based hourly products. The trends exhibited by the models were robust and showed little site dependency (Perez et al., 2011).

Here we address the issue of intraday variability with a variability time scale of one hour. For this purpose, the daily clear sky index is used as an input to infer the standard deviation of the changes in the hourly clear sky index over the considered day.

Previous studies (Stein et al., 2012; Kang and Tam, 2013) have demonstrated that it is possible to model intra-daily variability from ground-based solar radiation daily time series.

Stein et al. (2012) introduced a new metric: the variability index, VI, to quantify irradiance variability over various timescales. Three sites were used to evaluate the consistency of this new metric. By pairing the VI index with the daily clear sky index, KT^*, they showed that a characteristic scatter plot named the "arrow-head" plot emerged from the data at hand. A classification scheme based on the VI index and clear sky index was used to distinguish between four types of irradiance days.

In a similar manner, Kang and Tam (2013) proposed a new characterization and classification method (the K-POP method) for daily sky conditions by using the daily clearness index K_D and a new metric called the daily probability of persistence (POP_D). POP_D observes differences between neighboring instantaneous clearness indices and calculates a probability that the differences are equal to zero (Kang and Tam, 2013). Three sites were chosen to test the consistency of the method. The authors showed that the annual distribution of data points in the K-POP_D plane for all three locations were enclosed by the same irregular nonagon. From the K-POP_D plane the authors also identified 10 classes that correspond to different sky conditions.

In his thesis, Dambreville (2014) proposed a classification scheme based on the daily mean clear sky index and daily variability quantified by the V metric (Coimbra et al., 2013). The classification was used to characterize the sky conditions experienced by a site located near Paris.

Some authors (Huang et al., 2014; Kang and Tam, 2015) also went further by deriving some prediction models of daily variability. For instance, Huang et al. (2014) studied the daily variability at four sites across Australia by using the Daily Variability Index (DVI) – which is similar to the VI (Stein et al., 2012). In addition to the persistence model, they also built three statistical models (including a machine learning technique) to predict the DVI using meteorological variables as predictors. The latter were selected from the global atmospheric reanalysis product of the European Centre for Medium-Range Weather Forecasts (ECMWF). However, as noted by the authors in their conclusion, the probability density function (PDF) of the DVI was not well reproduced by the statistical techniques and may suggest a limitation of these techniques in tackling the solar variability problem.

Kang and Tam (2015) used the National Weather Service (NWS) day-ahead total sky cover forecast to predict the day-ahead K_D and POP_D values. A multi-stage procedure (including a robust regression technique) was employed to estimate the parameters of a linear equation relating the daily fluctuation of solar irradiance (POP_D) to the daily fluctuation of total sky cover. The forecasting method was tested on one year of data from the Solar Radiation Research Laboratory Baseline Measurement System (SRRL BMS). As noted by the authors, overall, the proposed method provides acceptable predictions results but further improvement is needed in the intermediate K_D zone that corresponds to the lowest POP_D values (or conversely to the highest variability values).

In this study, we make a step further by analyzing intra-day solar variability of twenty sites that exhibit different types of climate. For this purpose, we select 14 climatically distinct regions of North America as well as 6 subtropical/tropical island territories.

First, we propose a simple site characterization based on 2 criteria: (1) the daily clear sky index is used as an input to define a given day's meteorological conditions and (2) hourly intraday variability measured by a well-established metric – the standard deviation of the changes in the clear sky index (Perez and Hoff, 2013) – is used to quantify variability.

Second, based on a strong empirical evidence, we propose a parameterization of the intraday solar variability stating that intraday variability is a predictable function of daily clear sky index.

It must be stressed however that contrary to (Huang et al., 2014; Kang and Tam, 2015) our aim here is to propose a simple but yet effective and actionable approach.

Such a characterization would be helpful in an operational context. Predicted intraday variability enhances the informative content of day(s) ahead Numerical Weather Prediction (NWP) forecasts – operational forecasts such as ECMWF have a limited time resolution and tend to underestimate intraday dynamics. This information could be of particular relevance to grid operators' decision

making, particularly in non-interconnected insular networks. For instance, a predicted high variability day may suggest an adaptation of the operational planning with ready deployment of stand-by generation capability.

2. Metrics, model derivation and data

The two quantities used in the proposed parameterization are the daily clear sky index KT* (the variability predictor) and the intraday variability per se given by the standard deviation of the change in the clear sky index, over the considered day.

2.1. Daily clear sky index

The parameter used to characterize the daily solar conditions is the daily clear sky index (KT*). The daily clear index KT* is defined by:

$$\mathrm{KT}^* = \frac{\sum_{i=1}^{N_h} GHI(i)}{\sum_{1=1}^{N_h} GHI_{clear}(i)} \quad (1)$$

where N_h represents the number of daylight hours (i.e. for which the solar zenith angle SZA $< 85°$) in a day.

GHI is the hourly global horizontal irradiance and GHI_{clear} represents the clear sky global irradiance for the considered hour and can be obtained from (Bird and Hulstrom, 1981) or Ineichen, 2006). The Bird model (Bird and Hulstrom, 1981) was used for the six insular sites while the simplified SOLIS model (Ineichen, 2008) was used for the US locations, noting that the choice of model would have virtually no impact on the present observations.

2.2. Intraday variability

The intradaily variability is given by the standard deviation of the change in the clear sky index over the considered day i.e. $\sigma(\Delta kt^*_{\Delta t})$. (Perez et al., 2015) called this metric the nominal variability. Nominal variability refers to the variability of the dimensionless clear sky index kt^* which is directly correlated with the ramp rates' magnitude.

Other metrics have been proposed to characterize the variability (e.g., Perez et al., 2011; Coimbra et al., 2013). However, most authors prefer using the nominal variability over a given time span as the metric for variability. We retain this definition of nominal variability:

$$Nominal\ Variability = \sigma\left(\Delta kt^*_{\Delta t}\right) = \sqrt{Var\left[\Delta kt^*_{\Delta t}\right]} \quad (2)$$

In this application, the time scale $\Delta t = 1$ h and the time span is N_h hours.

Let us also recall that the clear sky index kt^* is defined as the ratio of GHI to clear sky GHI.

We also provide two complementary metrics: the maximum absolute clear sky index change occurring within the day i.e. $\max(|\Delta kt^*_{\Delta t}|)$ and the median absolute deviation (MAD) of the $(\Delta kt^*_{\Delta t})$ series for the considered day i.e. $mad[\Delta kt^*_{\Delta t}]$. These two metrics enhance the information contained in $\sigma(\Delta kt^*_{\Delta t})$. The first metric should be relevant for the grid operators as it quantifies an upper limit of the intraday variability while the second metric, contrary to the standard deviation, is less sensitive to extremes and/or outliers.

2.3. Model derivation and structure

As mentioned above, the objective of this paper is two-fold. First, it proposes a simple site characterization and second a model that parameterizes the intraday solar variability. Regarding the structure of the model, the known input to the model is the daily clear sky index. The unknown output of the model consists of the metric that estimates the site intraday variability $\sigma(\Delta kt^*_{\Delta t})$.

The model is built empirically from hourly GHI ground measurements at several climatically distinct locations. The model consists of one lookup table defined by KT* and returning the intradaily variability metric (the lookup table is given in section results).

2.4. Experimental data

Seven stations, part of NOAAA's SURFRAD network (SURFRAD, 2010), seven stations from the NOAA's ISIS network (ISIS, 2010), and six insular sites are selected for the empirical analysis. Each station provides one year of GHI observations at hourly time scale. This leads to a total of 7110 days or 170,640 hourly measurements. The experimental data are further detailed in Table 1.

Two locations have been chosen for the islands of La Reunion (Saint-Pierre – coastal site and Le Tampon-inland site) and Gran Canaria (Las Palmas and Pozo Izquierdo).

In the case of La Réunion, the two aforementioned sites are quite representative of a tropical island with a complex orography. Hence, although distant of only 10 km, these two sites exhibit very different sky conditions (Diagne, 2015).

For Gran Canaria island, we chose two representative stations that take into account the climatic variability of the island (Mazorra Aguiar et al., 2010). Pozo Izquierdo is situated in the south of the Island and presents a large amount of clear days, while Las Palmas, northern station, is affected by clouds formation during summer due to the trade winds effect.

3. Results

3.1. Site characterization

The proposed parameterization scheme delineates a 2-dimensional space illustrated in Fig. 1 for the site of Sterling. It is clear from this illustration that intraday variability is a robust function of the daily clear sky index,

Table 1
Sites under study.

Station	Latitude	Longitude	Elevation (m)	Climate	Year
Surfrad network					
Goodwin Creek	34.25	−89.87	98	Subtropical	2013
Desert Rock	36.63	−116.02	1007	Arid	2013
Bondville	40.05	−88.37	213	Continental	2013
Boulder	40.13	−105.24	1689	Semi-arid	2013
Penn State	40.72	−77.93	376	Humid continental	2013
Sioux Falls	43.73	−96.62	473	Continental	2013
Fort Peck	48.31	−105.10	634	Continental	2013
ISIS network					
Sterling	38.95	−77.45	85	Humid continental	2013
Seattle	47.65	−122.25	20	Temperate maritime	2013
Salt Lake City	40.75	−111.95	1288	Semi-arid	2013
Madison	43.15	−89.35	271	Continental	2013
Handford	36.35	−119.65	73	Mediterranean	2013
Bismarck	46.75	−100.75	503	Continental	2013
Albuquerque	35.05	−106.65	18	Subtropical	2013
Insular sites					
Raizet (Guadeloupe)	16.264	−61.516	11	Tropical	2012
Oahu (Hawaii)	21.312	−158.084	11	Tropical	2011
Saint-Pierre (Réunion)	−21.340	55.491	75	Tropical	2012
Tampon (Réunion)	−21.269	55.506	550	Tropical	2013
Pozo Izquierdo (Gran canaria)	27.817	−15.424	47	Subtropical	2005
Las Palmas (Gran Canaria)	28.110	−15.426	17	Subtropical	2005

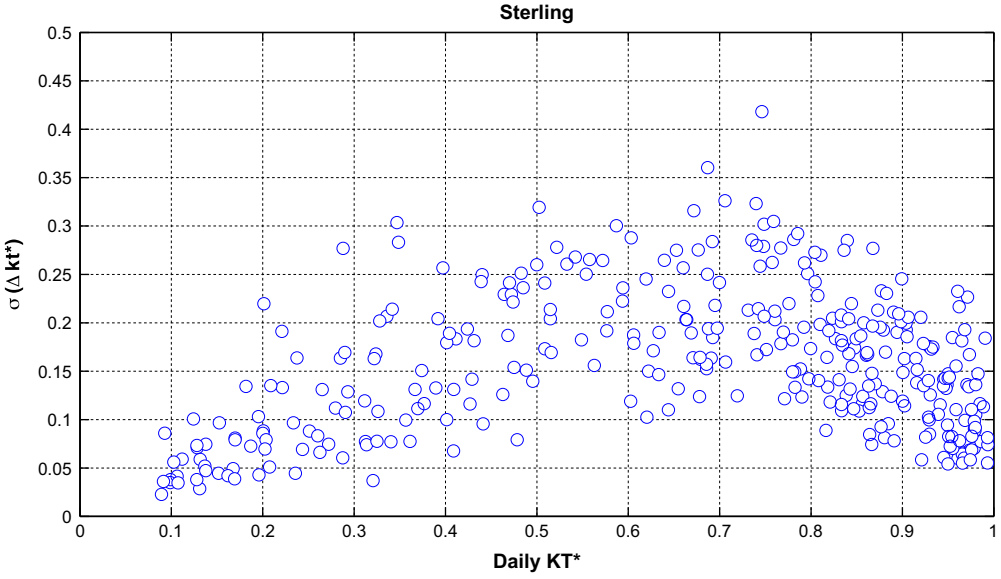

Fig. 1. Two-dimensional space KT^*–$\sigma(\Delta kt^*_{\Delta t})$ – Sterling site.

ranging from little to no variability for dark overcast and very clear conditions to maximum variability for intermediate conditions. Remarkably, the trend illustrated for Sterling is very similar to the trends observed at all other locations as shown in Fig. 2. Although the distribution of occurrences in the 2-dimensional space varies from location to location depending on climate (e.g., compare Desert Rock and Sterling) the trends linking KT^* and $\sigma(\Delta kt^*_{\Delta t})$ exhibit only a minor influence of the local climatic environment. These similarities as also noted by Stein et al. (2012) have a physical basis due to the cloud-induced fluctuations processes. Indeed, in a very interesting article, Reno and Stein (2013) showed that the variability represented either by the VI index or the standard deviation of the clear sky index time series was dependent upon the cloud category.

The composite $\sigma(\Delta kt^*_{\Delta t})$ vs. KT^* trend for all locations is shown in Fig. 3. The dark line represents the global mean trend calculated with data of all sites. This global mean trend was derived by taking the mean of the probability density of the variability for each bin of KT^*. This method

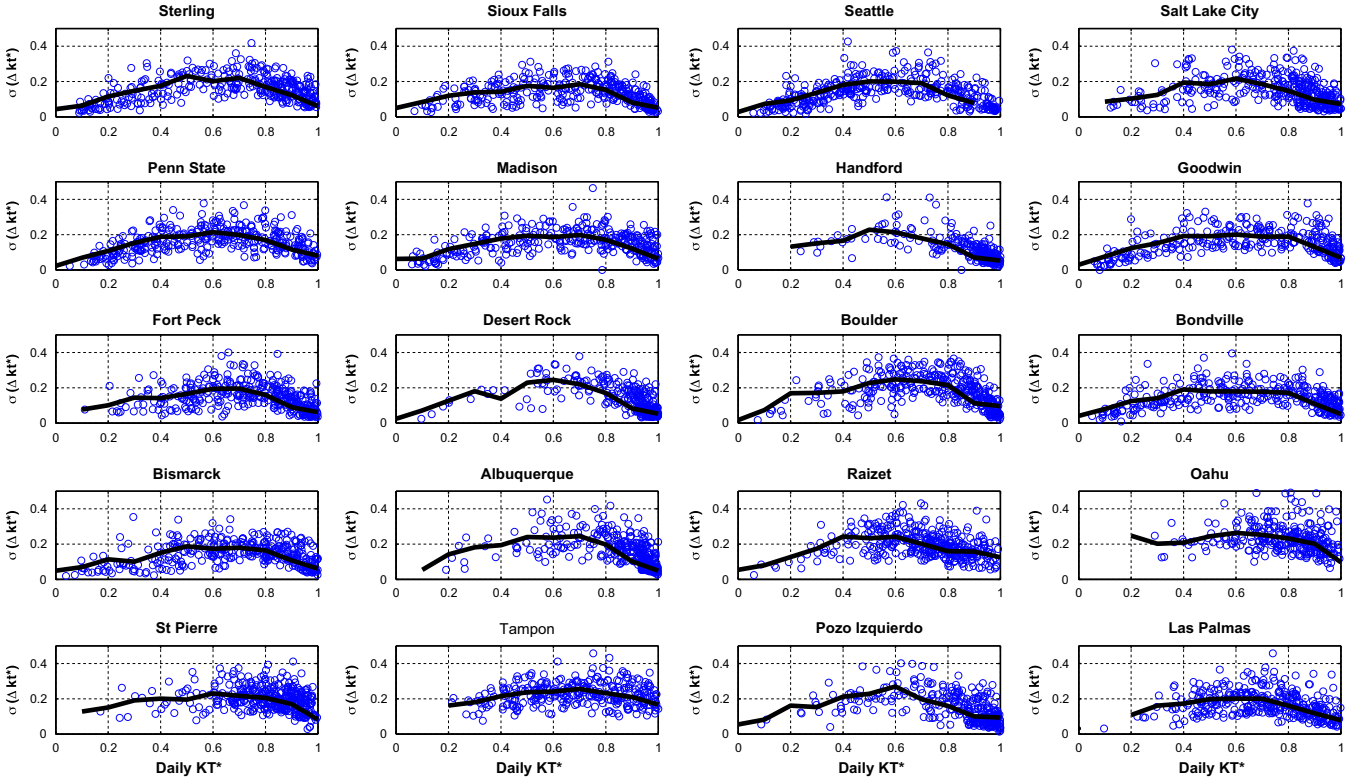

Fig. 2. Distribution of points in the plane KT^*–$\sigma(\Delta kt^*_{\Delta t})$ for all sites. The black line represents the mean trend of each site.

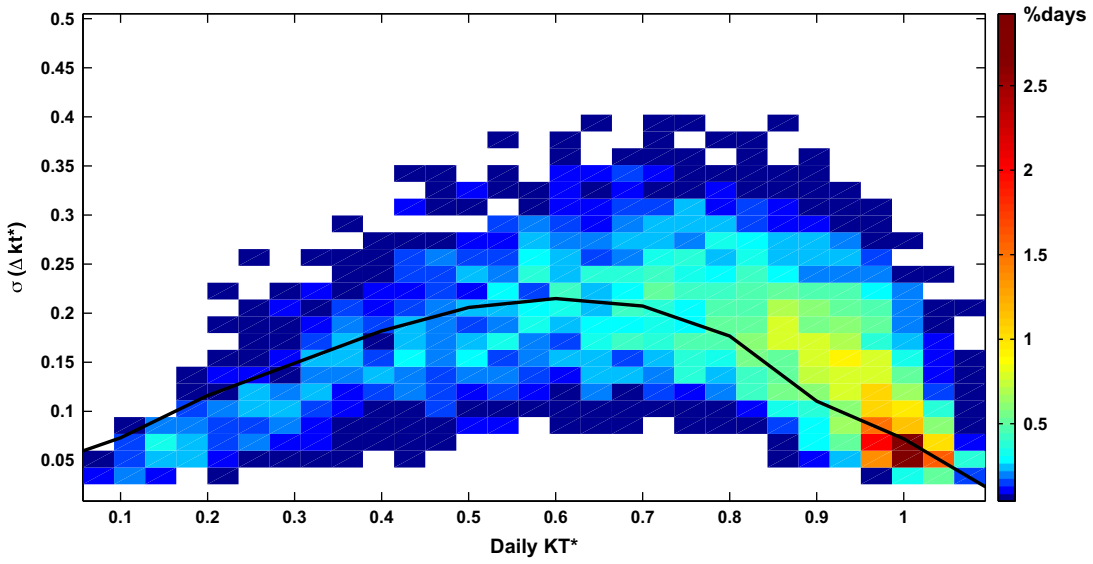

Fig. 3. Scatter density plot for all locations representing 7110 days. The black line represents the global mean trend.

was applied after checking that the distribution estimates were unimodal. This well-defined trend suggests that intra-daily variability can be conjectured from daily clear sky index.

In an attempt to explain the scattering of the data that appear in Figs. 1 and 2, similarly to (Huang et al., 2014), we did investigate the correlation between intra-day variability and other meteorological variables provided by ECMWF such as Total Cloud Cover (TCC), Air Temperature (AT), 700 hPa Geopotential (GP700), 850 hPa Geopotential (GP850), Cloud Base Height (CBH), Zonal wind velocity (U), Meridional wind velocity (V). Apart

TCC, which behaves very much like the daily clear sky index (KT*), none of these variables produced measurable correlations with the intra-day variability.

Individual site trends are intercompared in Fig. 4. Trends are comparable, but some differences are nevertheless apparent, with some locations systematically over the global trend and others systematically below the global trend. Fig. 5 present the trends obtained for the $\max(|\Delta kt^*_{\Delta t}|)$ metric.

Fig. 6 plots the average deviation between the global mean trend and each individual site's trend. This figure reveals that sites above the trend – Albuquerque, Boulder, both Reunion Island sites, Hawaii, Guadeloupe, and one of the Canary Islands site – tend to be sites where cloud buildup is influenced by nearby orography. The sites below the trend are locations where cloud regimes are driven primarily by the passage of weather systems. The one exception is Las Palmas, however this site is on the windward side of the island and often experience a low level stable cloud layer more representative of the ocean mass ahead unlike the typical orography-driven cloud build-up characterizing partly cloudy events at the other sites.

Although the individual trends do not deviate substantially from the average trend, suggesting that the proposed parameterization is robust, Figs. 7 and 8 propose two separate trends for sites where cloud regimes are, and are not influenced by orographic build up, denoted respectively as type B and type A.

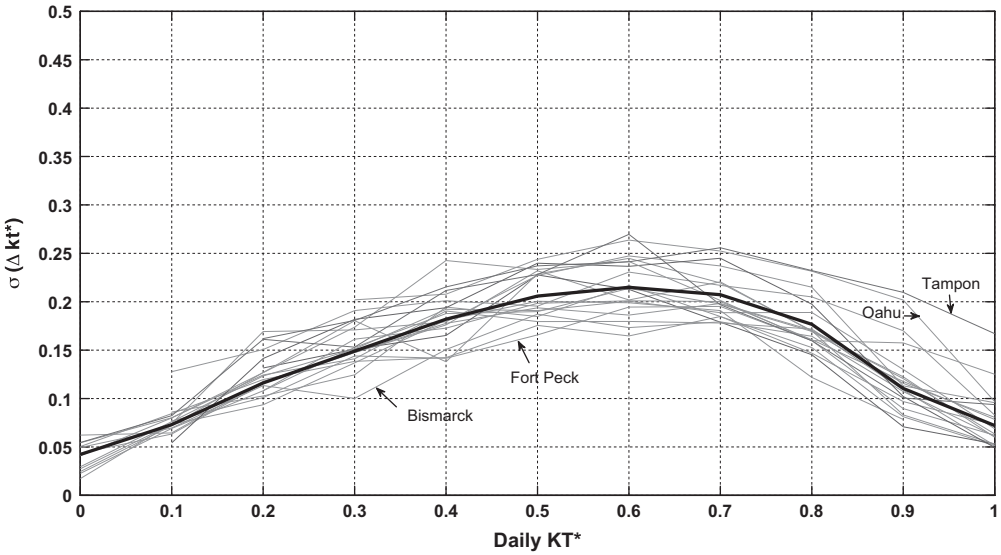

Fig. 4. Average trends of each site. The black line represents the global average trend.

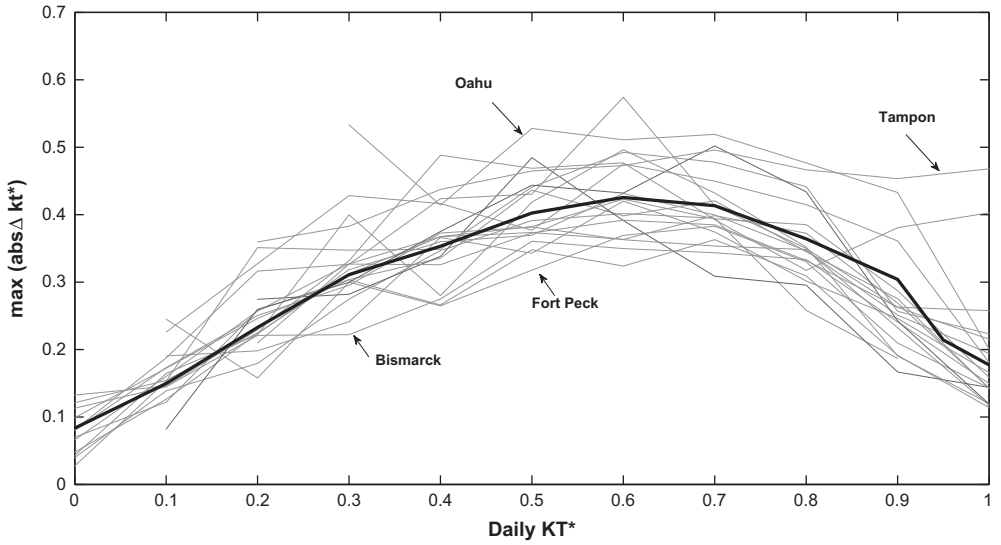

Fig. 5. Same as Fig. 4 but for the $\max(|\Delta kt^*_{\Delta t}|)$ metric.

Figs. 9 and 10 are analogous to Figs. 7 and 8, but present the trends calculated for the maximum clear sky index change metric i.e. $\max(|\Delta kt^*_{\Delta t}|)$.

3.2. Parameterization of intradaily variability

The above observations led us to propose a simple model that quantifies intraday variability as a function of the daily clear sky index.

Although it would be possible to fit a continuous function (say for instance a polynomial of order 4) to the data, we propose here a modeling approach based on a look-up conversion table. Indeed, this technique has proven effective both in the case of solar irradiation transposition models (Perez et al., 1990) and solar irradiation fluctuations models (Perez et al., 2011). The Lookup table is given in Table 2. Table 2 reports the three intraday variability metrics derived for all observations falling in a particular KT*

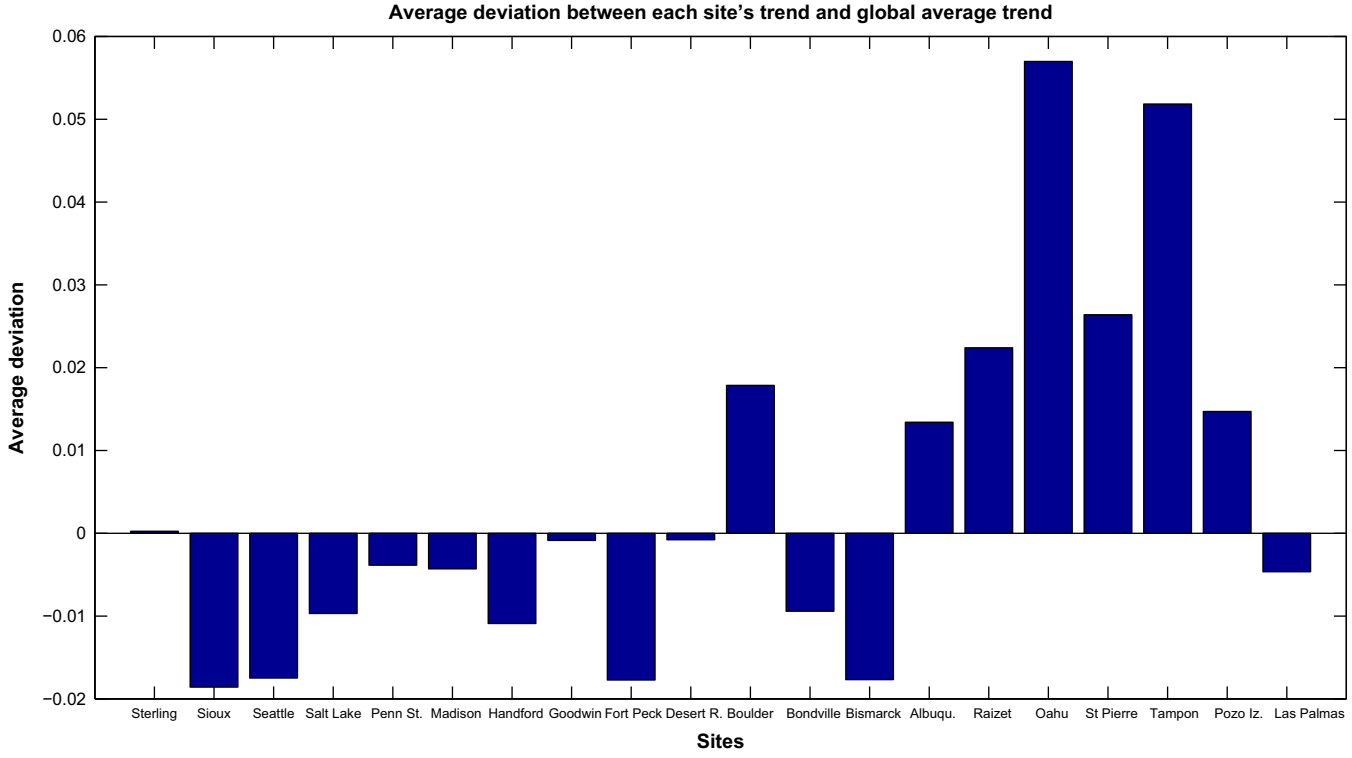

Fig. 6. Average deviation between each site's trend and global average trend.

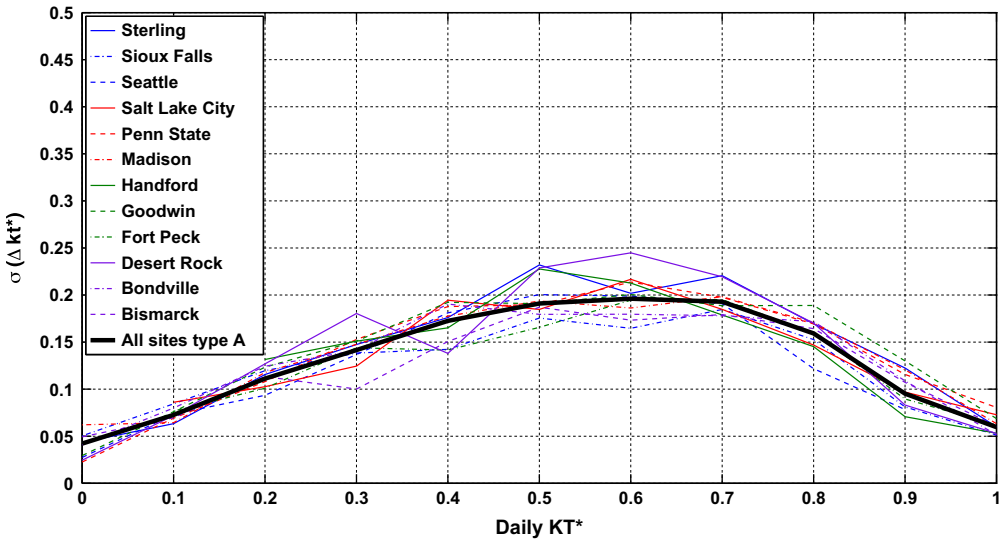

Fig. 7. Average trends for sites where cloud formation is traceable to weather events only. The black line represents the mean trend of the sites type A.

bin as well as the standard deviations around these means. The number of observations in each bin is also reported in Table 2. The number of observations should provide an indication of the robustness of any particular bin value. Tables 3 and 4 propose two complementary models for sites with cloud formations influenced by orography (type B) and sites where cloud formation is traceable to weather events only (type A).

3.3. Model application example: day-ahead forecasts paired with intradaily variability

Day ahead solar irradiance forecasting is essential for an efficient integration of large shares of solar energy into the electricity grid. In addition to the day ahead forecasts, an information related to the expected intraday variability could be a great help for the grid operator in such a context of decision-making. Day ahead forecasts are produced by numerical weather prediction (NWP) models (e.g., ECMWF). Although these forecasts are increasingly accurate (Perez et al., 2013) especially in terms of daily KT* prediction, they generally produce smoothed irradiance profiles and lack in hour to hour dynamics. Using the predicted KT*, one could apply the proposed parameterization (Table 2) to estimate intraday variability.

Fig. 11 shows the intraday variability inferred from the ECMWF forecasts at the site of Saint-Pierre with two variants. The first case (Fig. 11a) plots the predicted intraday

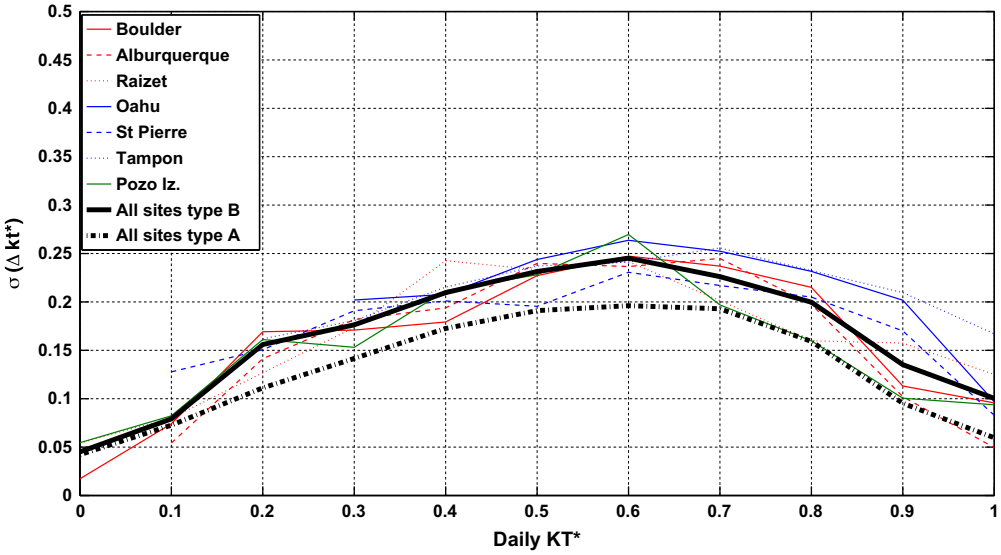

Fig. 8. Average trends for sites with cloud formations influenced by orography (type B). The black line represents the average trend of the concerned sites. For ease of comparison, we also add the average trend of sites type A as a dotted dark line.

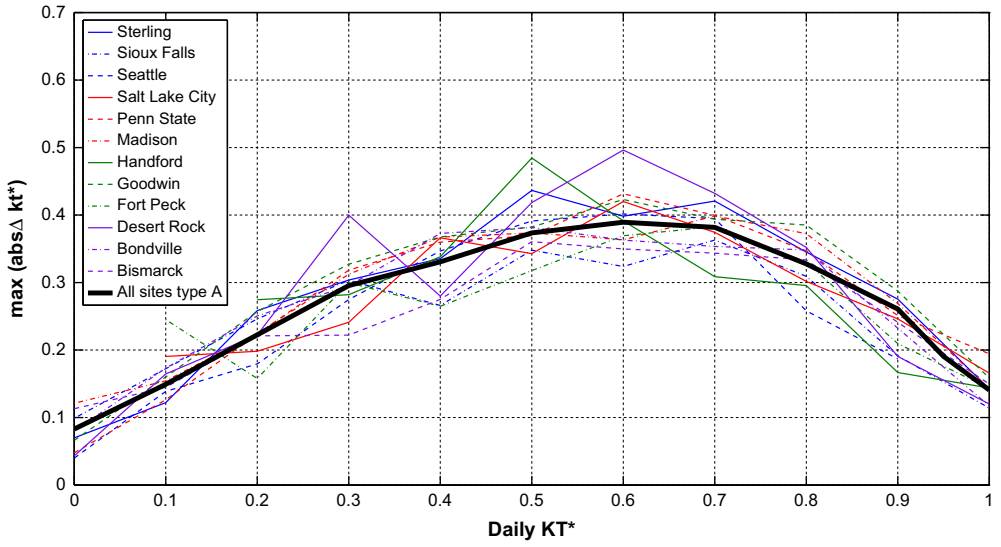

Fig. 9. Same as Fig. 7 but for the max($|\Delta kt^*_{\Delta t}|$) metric.

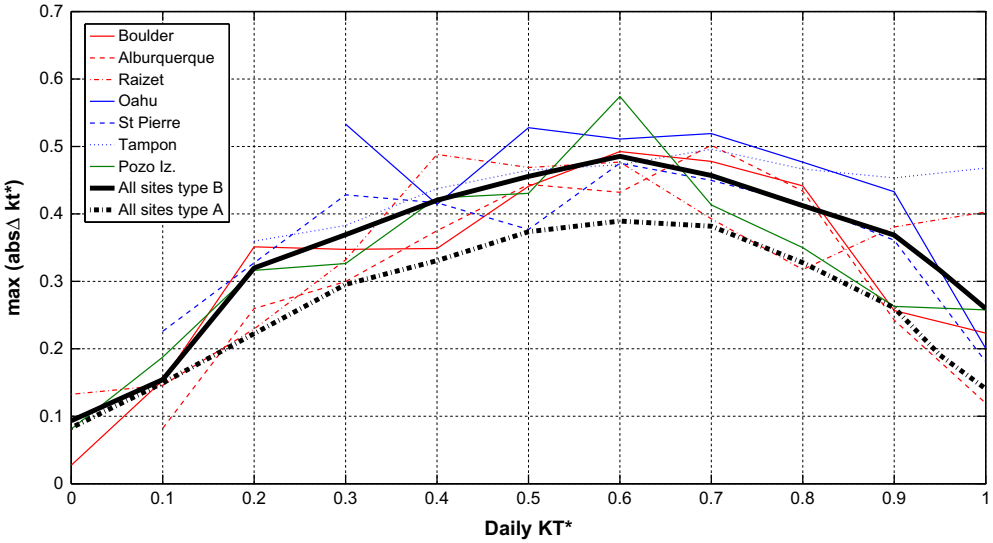

Fig. 10. Same as Fig. 8 but for the $\max(|\Delta kt^*_{\Delta t}|)$ metric.

Table 2
Lookup table global model.

KT^*	$\sigma(\Delta kt^*_{\Delta t})$	$\max(\lvert\Delta kt^*_{\Delta t}\rvert)$	$mad[\Delta kt^*_{\Delta t}]$	Number of observations
<0.1	0.04 ± 0.02	0.08 ± 0.05	0.03 ± 0.01	42
0.1–0.2	0.07 ± 0.04	0.15 ± 0.10	0.05 ± 0.02	192
0.2–0.3	0.11 ± 0.06	0.23 ± 0.13	0.09 ± 0.04	256
0.3–0.4	0.15 ± 0.06	0.31 ± 0.14	0.11 ± 0.04	320
0.4–0.5	0.18 ± 0.07	0.35 ± 0.15	0.14 ± 0.05	464
0.5–0.6	0.20 ± 0.07	0.40 ± 0.15	0.15 ± 0.05	545
0.6–0.7	0.21 ± 0.07	0.42 ± 0.16	0.16 ± 0.05	712
0.7–0.8	0.20 ± 0.07	0.41 ± 0.15	0.15 ± 0.05	863
0.8–0.9	0.17 ± 0.07	0.36 ± 0.15	0.13 ± 0.05	1236
0.9–0.95	0.14 ± 0.07	0.30 ± 0.16	0.10 ± 0.04	851
0.95–1	0.09 ± 0.06	0.21 ± 0.14	0.06 ± 0.03	1125
<1.1	0.07 ± 0.05	0.18 ± 0.13	0.05 ± 0.03	506

Table 3
Lookup table model for sites with cloud formations influenced by orography (type B).

KT^*	$\sigma(\Delta kt^*_{\Delta t})$	$\max(\lvert\Delta kt^*_{\Delta t}\rvert)$	$mad[\Delta kt^*_{\Delta t}]$	Number of observations
<0.1	0.05 ± 0.03	0.10 ± 0.08	0.03 ± 0.02	4
0.1–0.2	0.08 ± 0.03	0.16 ± 0.08	0.06 ± 0.02	12
0.2–0.3	0.16 ± 0.06	0.32 ± 0.16	0.12 ± 0.04	28
0.3–0.4	0.18 ± 0.06	0.37 ± 0.17	0.13 ± 0.04	62
0.4–0.5	0.21 ± 0.07	0.42 ± 0.15	0.16 ± 0.05	118
0.5–0.6	0.23 ± 0.07	0.46 ± 0.17	0.17 ± 0.05	192
0.6–0.7	0.25 ± 0.07	0.48 ± 0.16	0.18 ± 0.05	267
0.7–0.8	0.23 ± 0.07	0.46 ± 0.15	0.17 ± 0.05	359
0.8–0.9	0.20 ± 0.07	0.41 ± 0.16	0.14 ± 0.05	531
0.9–0.95	0.16 ± 0.07	0.37 ± 0.17	0.11 ± 0.05	340
0.95–1	0.11 ± 0.07	0.26 ± 0.17	0.07 ± 0.04	375
<1.1	0.10 ± 0.06	0.26 ± 0.17	0.06 ± 0.04	152

variability in case of a perfect forecast of the daily KT^* (i.e. forecasted KT^* = measured KT^*) while Fig. 11b displays the case where both KT^* and intraday variability are inferred from the ECMWF forecasts. In Fig. 11, intraday variability points are randomly drawn from a Gaussian distribution whose mean and standard deviation are given by the look-up table. In this example, we simply used the look-up table given by Table 2 which represents the 'general' model. Since this example is for the site of Saint-Pierre (Réunion island), one could have used Table 3 (local

Table 4
Lookup table model for sites where cloud formation is traceable to weather events only (type A).

KT^*	$\sigma(\Delta kt^*_{\Delta t})$	$\max(\lvert\Delta kt^*_{\Delta t}\rvert)$	$mad[\Delta kt^*_{\Delta t}]$	Number of observations
<0.1	0.04 ± 0.02	0.08 ± 0.05	0.03 ± 0.01	37
0.1–0.2	0.07 ± 0.04	0.15 ± 0.09	0.05 ± 0.03	180
0.2–0.3	0.11 ± 0.06	0.22 ± 0.13	0.08 ± 0.04	223
0.3–0.4	0.14 ± 0.06	0.29 ± 0.13	0.10 ± 0.04	245
0.4–0.5	0.17 ± 0.07	0.33 ± 0.14	0.13 ± 0.05	313
0.5–0.6	0.19 ± 0.06	0.37 ± 0.13	0.14 ± 0.05	310
0.6–0.7	0.20 ± 0.06	0.39 ± 0.14	0.15 ± 0.05	387
0.7–0.8	0.19 ± 0.06	0.38 ± 0.14	0.14±0.05	441
0.8–0.9	0.16 ± 0.06	0.32 ± 0.13	0.12 ± 0.04	644
0.9–0.95	0.12 ± 0.05	0.26 ± 0.13	0.08 ± 0.04	475
0.95–1	0.08 ± 0.04	0.19 ± 0.12	0.05 ± 0.03	724
<1.1	0.06 ± 0.03	0.14 ± 0.08	0.04 ± 0.02	349

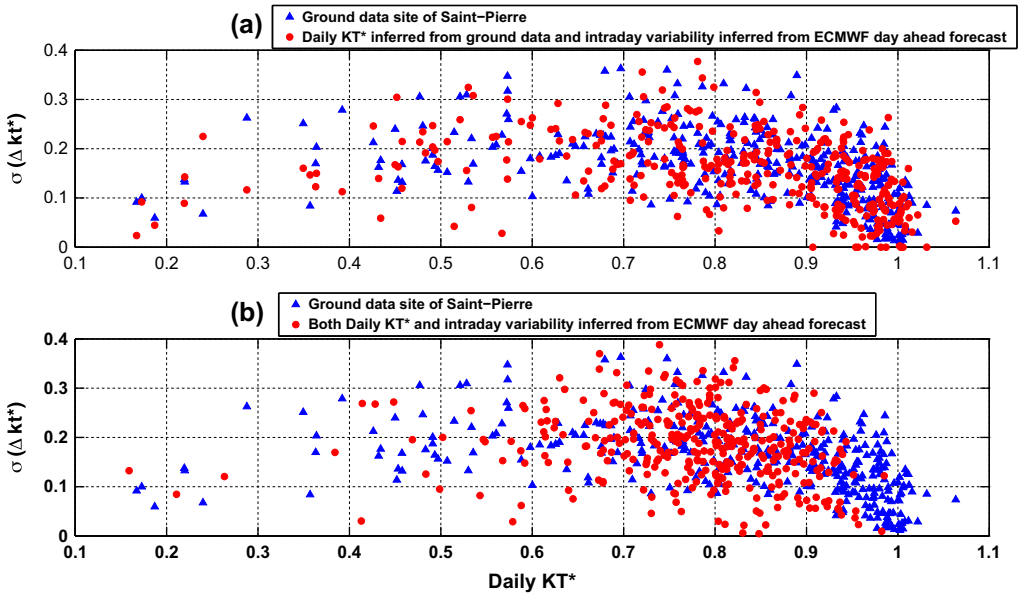

Fig. 11. Intradaily variability inferred from day-ahead ECMWF forecasts.

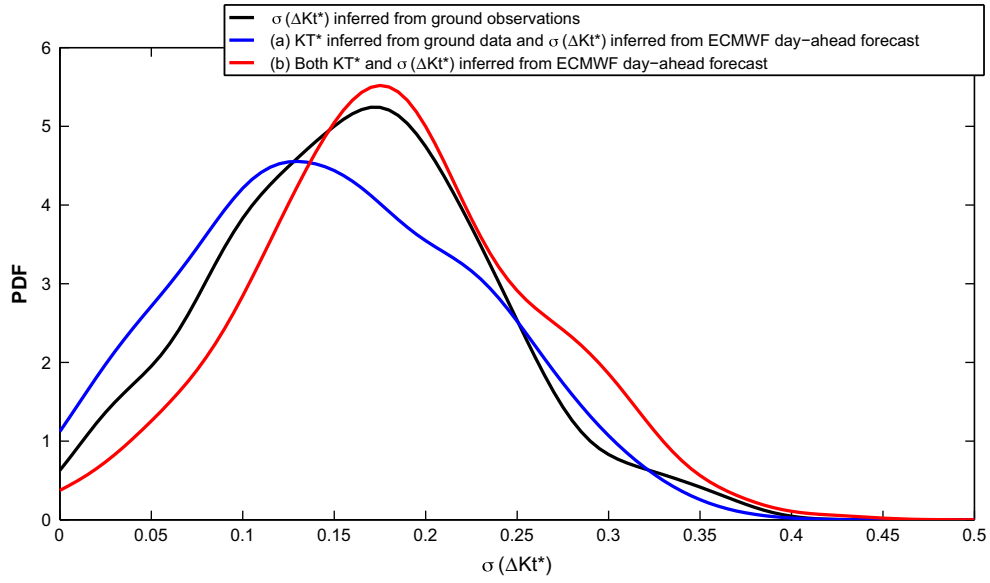

Fig. 12. PDFs of the intraday variability $\sigma(\Delta kt^*_{\Delta t})$.

orographic influence) but this would not fundamentally change our illustrative example. Fig. 11a shows the performance of the proposed model in the ideal case of a perfect forecast of KT^*. As seen, the model reproduces quite well the density of the measured variability. In an operational environment where KT^* is predicted with a degree of uncertainty (day-ahead ECMWF for the purpose of illustration), Fig. 11b shows that the proposed parameterization could be valuable; indeed the most interesting zone that corresponds to the maximum variability (intermediate KT^* values) is rather well reproduced. Future improvements of NWP forecasts will make Fig. 11b tend to Fig. 11a.

In order to quantitatively illustrate the previous statements, Fig. 12 plots the probability density functions (PDFs) of the $\sigma(\Delta kt^*_{\Delta t})$ for the site of St Pierre resulting from the application of our method. As seen, the PDFs (cases (a) and (b) of Fig. 11) are comparable to the PDF of the $\sigma(\Delta kt^*_{\Delta t})$ ground observations.

4. Conclusions

We presented a site characterization based on 2 parameters: the daily clear sky index KT^* and the intraday variability given by a commonly accepted metric: the standard deviation of the changes in the clear sky index $\sigma(\Delta kt^*_{\Delta t})$ We showed that the relationship between these two quantities had little dependence on location – suggesting that intraday variability could be inferred from the day's mean clear sky index. However we noted some influence on the relationship that could be traced on a site's orography and its influence on cloud formation. Sites where orographic cloudiness might be expected tend to exhibit more variability for a given mean daily clear index than sites where cloud regimes are driven by weather.

We used the empirical evidence assembled from 20 locations to propose a simple model to infer intraday variability from a day's clear sky index. Such a simple model could be used to enhance the informative content of day(s) ahead NWP forecasts.

Acknowledgments

The authors would like to thank the European Centre for Medium-Range Weather Forecasts (ECMWF) for providing forecast data.

The authors are very grateful to Canary Islands Technology Institute (Instituto Tecnológico de Canarias, I.T.C.) for providing ground measurements databases.

References

Badosa, J., Haeffelin, M., Chepfer, H., 2013. Scales of spatial and temporal variation of solar irradiance on reunion Tropical Island. Sol. Energy 88, 42–56.

Bird, R.E., Hulstrom, R.L., 1981. Simplified the clear sky model for direct and diffuse insolation on horizontal surfaces. In: Technical Report No. SERI/TR-642-761, Golden, CO, Solar Energy Research Institute.

Coimbra, C.F.M., Kleissl, J., Marquez, R., 2013. Overview of solar forecasting methods and a metric for accuracy evaluation. In: Kleissl, J. (Ed.), Solar Energy Forecasting and Resource Assessment. Elsevier, pp. 171–194.

Dambreville, R., 2014. Prévision du rayonnement solaire global par télédétection pour la gestion de la production d'énergie photovoltaïque. PhD thesis, Université de Grenoble.

Diagne, H.M., 2015. Gestion intelligente du réseau électrique Réunionnais. Prévision de la ressource solaire en milieu insulaire. PhD thesis, Université de La Réunion.

Hansen, T., 2007. Utility solar generation valuation methods, USDOE Solar America Initiative Progress Report. Tucson Electr. Power, Tucson, AZ.

Huang, J., Troccoli, A., Coppin, P., 2014. An analytical comparison of four approaches to modelling the daily variability of solar irradiance using meteorological records. Renew. Energy 72, 195–202.

Ineichen, P., 2006. Comparison of eight clear sky broadband models against 16 independent data banks. Sol. Energy 80, 468–478.

Ineichen, P., 2008. A broadband simplified version of the SOLIS clear sky model. Sol. Energy 82, 758–762.

ISIS, 2010. <http://www.esrl.noaa.gov/gmd/grad/isis/.

Kang, B.O., Tam, K.S., 2013. A new characterization and classification method for daily sky conditions based on ground-based solar irradiance measurement data. Sol. Energy 94, 102–118.

Kang, B.O., Tam, K.S., 2015. New and improved methods to estimate day-ahead quantity and quality of solar irradiance. Appl. Energy 13, 240–249.

Lave, M., Kleissl, J., Arias-Castro, E., 2012. High-frequency irradiance fluctuations and geographic smoothing. Sol. Energy 86, 2190–2199.

Lenox, C., Nelson, L., 2010. Variability comparison of large-scale photovoltaic systems across diverse geographic climates. In: 25th European Photovoltaic Solar Energy Conference, 6–10 September, Valencia, Spain.

Marcos, J., Marroyo, L., Lorenzo, E., Alvira, D., Izco, E., 2011. Power output fluctuations in large scale PV plants: one year observations with one second resolution and a derived analytic model. Prog. Photovolt. Res. Appl. 19, 218–227.

Mazorra Aguiar, L., Díaz, F., Montero, G., Montenegro, R., 2010. Typical Meteorological Year (TMY) Evaluation for Power Generation in Gran Canaria Island. In: 25th European Photovoltaic Solar Energy Conference, 6–10 September, Valencia, Spain.

Mills, A., Ahlstrom, M., Brower, M., Ellis, A., George, R., Hoff, T., Kroposki, B., Lenox, C., Nicholas, M., Stein, J., Wan, Y.W., 2010. Understanding Variability and Uncertainty of Photovoltaics for Integration with the Electric Power System. Lawrence Berkeley Natl. Lab.

Murata, A., Yamaguchi, H., Otani, K., 2009. A method of estimating the output fluctuation of many photovoltaic power generation systems dispersed in a wide area. Electr. Eng. Jpn. 166, 9–19.

Perez, R., Hoff, T., 2013. Solar resource variability. In: Kleissl, J. (Ed.), Solar Energy Forecasting and Resource Assessment. Elsevier, pp. 133–148.

Perez, R., Ineichen, P., Seals, R., Michalsky, J., Stewart, R., 1990. Modeling daylight availability and irradiance components from direct and global irradiance. Sol. Energy 44, 271–289.

Perez, R., Kivalov, S., Schlemmer, J., Hemker, K., Hoff, T., 2011. Parameterization of site-specific short-term irradiance variability. Sol. Energy 85, 1343–1353.

Perez, R., Lorenz, E., Pelland, S., Beauharnois, M., Van Knowe, G., Hemker Jr., K., Heinemann, D., Remund, J., Müller, S.C., Traunmüller, W., Steinmauer, G., Pozo, D., Ruiz-Arias, J.A., Lara-Fanego, V., Ramirez-Santigosa, L., Gaston-Romero, M., Pomares, L.M., 2013. Comparison of numerical weather prediction solar irradiance forecasts in the US, Canada and Europe. Sol. Energy 94, 305–326.

Perez, R., David, M., Hoff, T., Kivalov, S., Kleissl, J., Lauret, P., Perez, M., 2015. Spatial and temporal variability of solar energy. Foundations and Trends in Renewable Energy (forthcoming).

Perpiñán, O., Marcos, J., Lorenzo, E., 2013. Electrical power fluctuations in a network of DC/AC inverters in a large PV plant: relationship between correlation, distance and time scale. Sol. Energy 88, 227–241.

Reno, M.J., Stein, J.S., 2013. Using cloud classification to model solar variability. ASES National Solar Conference, April 16–20, 2013, Baltimore, Maryland.

Sengupta, M., Keller, J., 2011. PV ramping in a distributed generation environment: a study using solar measurements. IEEE Photovolt. Spec. Conf., 586–589

Stein, J.S., Hansen, C.W., Reno, M.J., 2012. The variability index: a new and novel metric for quantifying irradiance and PV output variability. World Renewable Energy Forum, 13–17 May 2012, Denver, Colorado.

SURFRAD Network, 2010. Monitoring Surface Radiation in the Continental United States. <http://www.esrl.noaa.gov/gmd/grad/surfrad/index.html.

Van Haaren, R., Morjaria, M., Fthenakis, V., 2014. Empirical assessment of short-term variability from utility-scale solar PV plants. Prog. Photovol. Res. Appl. 22, 548–559.